

Article

Seismic Vulnerability and Consolidation by FRP/FRCM Systems of a Masonry School Building in the District of Naples

Assunta Paola Piccolo ¹, Giovanna Longobardi ²  and Antonio Formisano ^{2,*} ¹ Olympus S.r.l., Via Riviera Di Chiaia 118, 80122 Napoli, Italy² Department of Structures for Engineering and Architecture, School of Polytechnic and Basic Sciences, University of Naples "Federico II", Piazzale Tecchio 80, 80125 Naples, Italy

* Correspondence: antoform@unina.it

Abstract: The paper discusses the seismic vulnerability of structures susceptible to overcrowding due to their intended use. Specifically, it addresses the analysis towards earthquake actions of a masonry school located in the Municipality of San Giorgio a Cremano, within the neighbourhood of Naples, providing different reinforcement interventions to ensure its seismic consolidation. After a brief introduction, the description of the analysis representative of the current condition of the structure is performed considering both static and seismic actions. The analysis results determine the seismic risk class of the building, allowing to identify its deficiencies, so to design structural consolidation interventions following the standard code indications. In particular, two retrofit techniques, namely, FRP and FRCM systems, are proposed with the purpose to evaluate their benefits to the school building from a seismic viewpoint. Finally, a comparison between the proposed intervention techniques is made to establish which one guarantees the best upgrading of the seismic condition of the examined building.

Keywords: seismic vulnerability; masonry building; static analysis; kinematic analysis; pushover analysis; consolidation operations; FRP system; FRCM systems



Citation: Piccolo, A.P.; Longobardi, G.; Formisano, A. Seismic Vulnerability and Consolidation by FRP/FRCM Systems of a Masonry School Building in the District of Naples. *Buildings* **2022**, *12*, 2040. <https://doi.org/10.3390/buildings12112040>

Academic Editor: Chisari Corrado

Received: 25 August 2022

Accepted: 9 November 2022

Published: 21 November 2022

Publisher's Note: MDPI stays neutral with regard to jurisdictional claims in published maps and institutional affiliations.



Copyright: © 2022 by the authors. Licensee MDPI, Basel, Switzerland. This article is an open access article distributed under the terms and conditions of the Creative Commons Attribution (CC BY) license (<https://creativecommons.org/licenses/by/4.0/>).

1. Introduction

Most of the existing building heritage is made of load-bearing masonry systems that are often in worrying conditions. This is due to the natural decay of materials' mechanical properties and their changing conditions, such as increased loads on the constructions. For these reasons, to prevent significant damage, it is necessary to intervene on these structures by performing consolidation interventions. From classic to traditional techniques, there are different ways to intervene on these buildings to guarantee their use and functionality.

In addition, since Italy is a high-seismicity area, these consolidating operations have to be performed as soon as possible so as to avoid possible damage to the built heritage under the occurrence of future catastrophic events.

Figure 1 represents the seismic hazard map of the Italian peninsula, which was delivered in 2001. Four zones have been individuated and numbered from the most (Zone 1) to the least dangerous (Zone 4). Each zone is identified according to the maximum value of the attended peak ground acceleration.

In particular, Figure 2 shows that the Campania region and the Neapolitan area, where the case study school herein inspected is placed, falls partially in Zone 1 and partially in Zone 2, so there is a high probability of occurrence of a strong earthquake in this territory.

Among the different ways to intervene on existing buildings, in the last years, fibre-reinforced composite materials have found numerous applications in different fields of engineering.

Despite this, the first applications in the construction field took place only after the eighties due to the uncertainties and doubts that the products' high cost and high technological content caused among the designers.

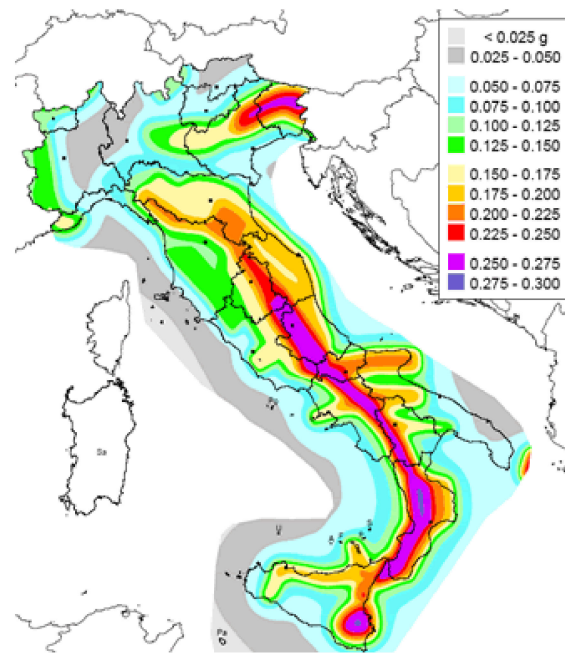


Figure 1. Seismic hazard map of Italy (National Institute of Geophysics and Volcanology, 2006).

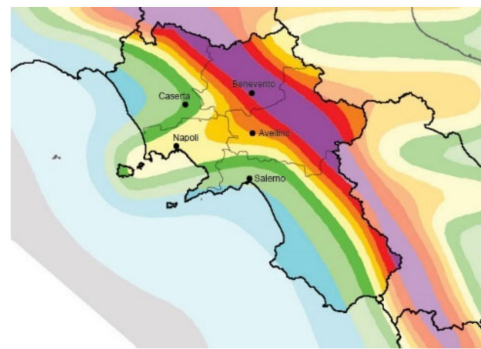


Figure 2. Detail of the seismic hazard of the Campania region of Italy (Darkest colour are the highest seismic zones).

However, the last decades have seen a rapid and sudden growth in the use of these systems, which, thanks to their numerous properties, today constitute a valid alternative to the use of classic traditional techniques in the seismic improvement and adaptation interventions. This growth is due not only to the increase in knowledge, as a result of a more significant number of laboratory experiments and the succession of multiple seismic events (such as the one that struck the Marche and Umbria in 1997 or that occurred in Central Italy in 2016), which have highlighted the true potential of reinforcement systems [1], but also to the enactment, starting from 2015, of a series of Standards and Guidelines [2] necessary to ascertain the identification, qualification and acceptance control of composites.

There are different types of composite systems. They all use a combination of two materials: a fibrous system for tensile strength and a matrix designed to guarantee adhesion to the support and impregnation. Precisely, concerning the matrix, it is possible to distinguish two categories of composite materials:

- FRP—Fibre-Reinforced Polymer: a technique that has spread rapidly thanks to the boost of economic convenience and the effectiveness demonstrated during the powerful Japanese and American earthquakes on the Pacific coast.
- FRCM—Fibre-Reinforced Cementitious Matrix: a more recent technique that is also widely used, mainly due to numerous applications and better knowledge of the

components. It is characterized by an inorganic matrix that contributes to greater environmental sustainability.

Both materials have excellent mechanical characteristics to be exploited for any intervention on masonry and reinforced concrete structures [3–18]. Thus, it is possible to affirm that innovative techniques can be integrated with classic ones in the same intervention. However, while traditional methods allow to strengthen the structures by increasing their strength and stiffness, modern ones, using lighter materials with reduced thickness, permit to achieve the same result without changing the structural stiffness. In addition, their use is highly advantageous, especially regarding the speed of application on-site and the low intrusiveness, resulting in being very advantageous in the case of applications in the cultural heritage field.

In the following sections, the performances of these two materials have been compared to each other through their application as retrofit technique of a case study represented by a masonry school building.

2. Knowledge Phase of the Case Study Building

The building under study is the Massaia Institute, located in the midpoint of the urban agglomeration of the municipality of San Giorgio a Cremano (Figure 3), in the province of Naples.

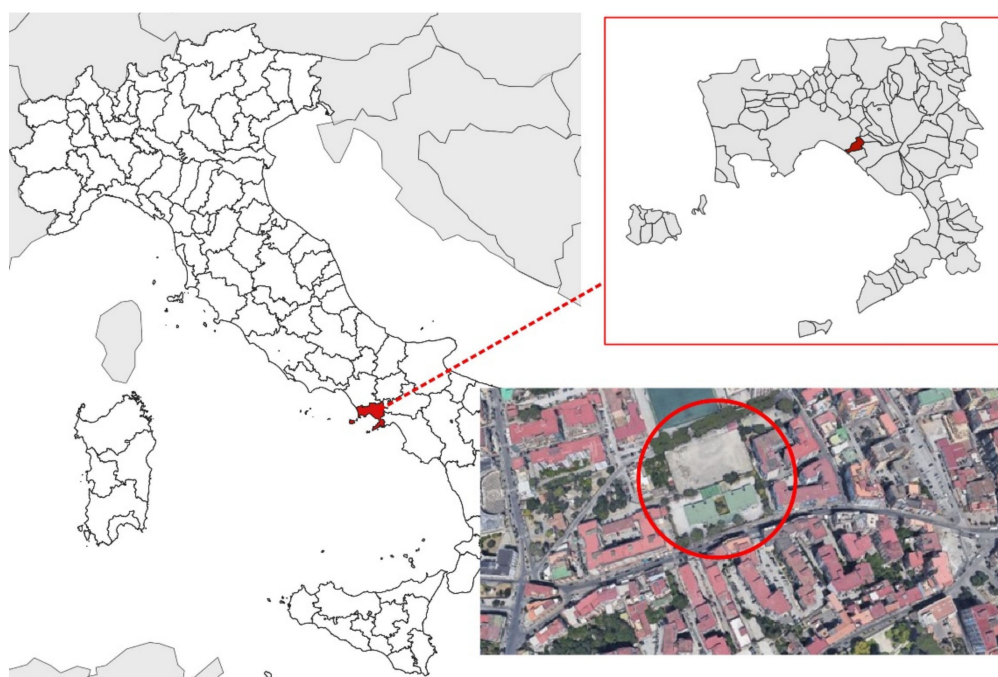


Figure 3. Placement of the school examined in San Giorgio a Cremano, Naples (Red circle indicates the school).

The building, used as secondary school, was designed by Engineer Francesco Santoli in 1965, under the auspices of the Law No. 645 of 9 August 1954. The building occupies a total area of 1650 square meters and consists of two distinct structures (Figure 4):

Body A: Main building developed on two levels above ground and made of load-bearing brick masonry and mixed reinforced concrete-tile floors, which is used as a school complex.

Body B: Reinforced concrete building consisting of a single floor for the portion used as gym and two floors above ground for the caretaker's home area.

The significant plan layouts of the two storeys of the building complex are shown in Figures 5 and 6.



Figure 4. Top view of the school's plexus (Google Maps, 2021).

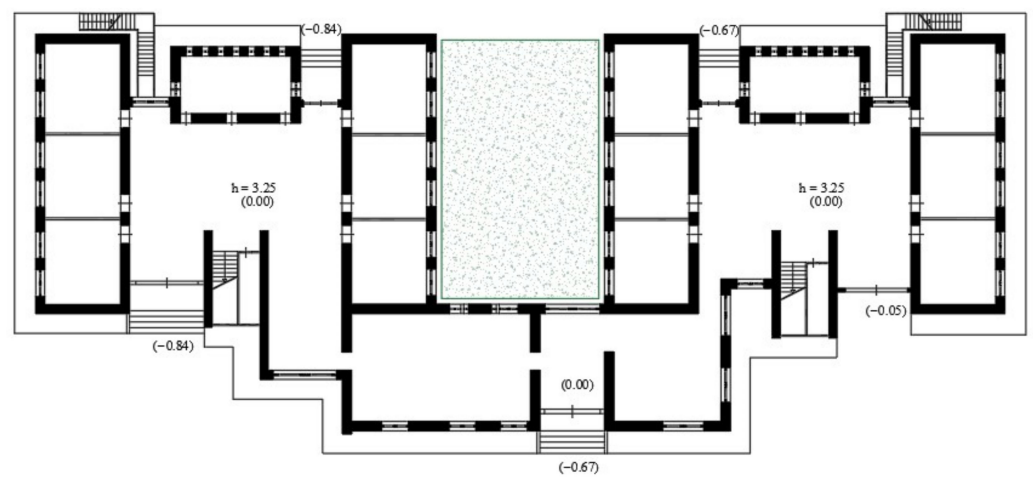


Figure 5. First level plan layout.

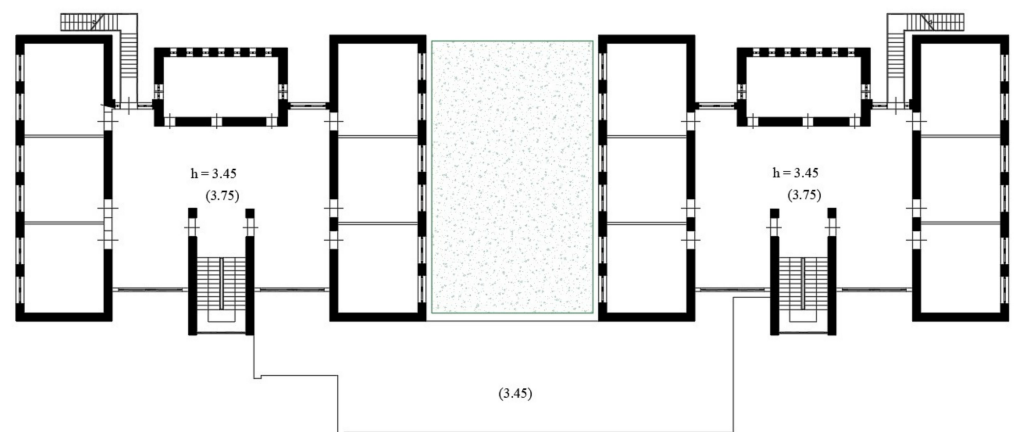


Figure 6. Second level plan layout.

In the current paper, the attention is devoted to Body A only.

The school, which has an articulated architectural configuration, is composed of rooms with different use, such as classrooms, laboratories, multimedia classroom, library, refectories, medical, toilets and an inner courtyard with a garden. Some pictures of the school facades taken during in situ surveys are shown in Figures 7 and 8.



Figure 7. The entrance of the school “Massaia”.



Figure 8. Some internal courtyard/garden views.

To reconstruct the geometrical and structural configuration of the structure, a geometric and material survey of the entire school complex was conducted, keeping in mind the quality and state of conservation of the vertical and horizontal structures.

To acquire the desired information, a visual survey was created and previous instrumental investigations, both non-destructive and partially destructive, were considered to ascertain the characteristics of the individual structural elements, their homogeneity and the quality of connections.

The tests conducted for mechanical characterization of masonry have foreseen thermographic investigations on floors for definition of their composition, excavations on foundations to define their typology, removal of plaster on load-bearing walls to determine the connection degree with floors and other walls and double flat jack tests. Illustrations of the different tests on structural components herein taken into consideration are found in Figures 9–13.

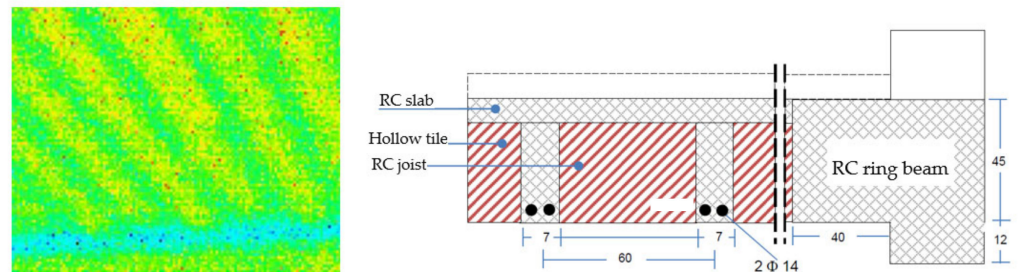


Figure 9. Ground level floor made of RC joists and tiles.

Based on these tests, as well as on the analysis of the structural details and properties of the materials, the building knowledge level can be considered as extensive.

From the performed surveys, it has been recorded that the building has an irregular in-elevation configuration, consisting of a portion (entrance zone) on one floor above ground and the remaining part with two floors above ground.



Figure 10. First level ribbed floor.

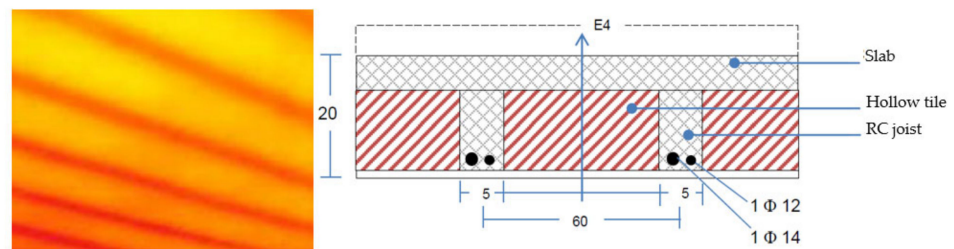


Figure 11. Mixed RC joists-hollow tiles floor at first level.



Figure 12. Corner detail and flat jack test of masonry walls made of Neapolitan yellow tuff stones.

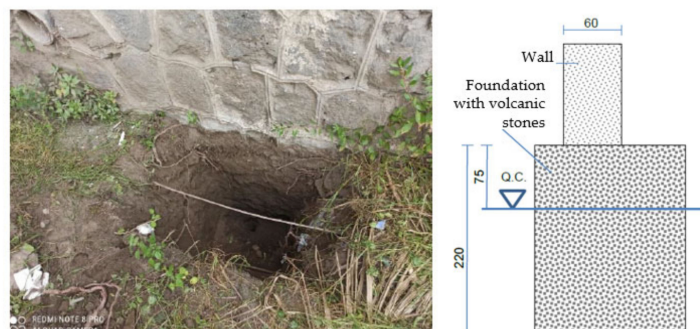


Figure 13. Investigation on foundation.

The supporting structure of the building consists of yellow tuff masonry walls with variable thickness between 55 cm and 65 cm and, generally, with a good degree of clamping among orthogonal walls.

The floors are made of on-site casted RC joists at both ground and first level floors. Connection between floors and walls is established through RC ring beams of width equal to the thickness of masonry walls.

The foundations, consisting of volcanic stones, are of direct type with height of about 220 cm. They are in good conditions, since, from the tests and inspections performed, no signs of instability due to settlements were detected.

2.1. Mechanical Characterization of Materials

According to previous investigations performed on the structure, the masonry types have been identified in two categories, namely, split masonry with stones assembled with good texture and soft stone masonry made of tuff bricks. For this latter category, masonry properties were obtained from in situ tests. In contrast, for the former masonry category, mechanical properties were obtained from Table C8.5.I of the Italian Circular No. 7/2019 considering medium values of the ranges defined for both resistance and elastic modulus.

In this case, since the mortars' characteristics are not available, the standard tabular values are assumed, to stay on the safe side, without the corrective coefficients for improvement of the masonry's seismic behaviour.

Based on the detailed geometric survey and the extended existing verifications of materials properties, a Level of Knowledge 2 (LC2) is considered reached for masonry in elevation, whereas LC1 is used to characterize foundation masonry. In particular, a flat jack test is performed on masonry walls of the school building, providing the data reported in Table 1.

Table 1. Results of the flat jack test.

| Feature | Value |
|-----------------------------------|------------------------------|
| Compression Strength–1st Cracking | $f_m = 1.10 \text{ N/mm}^2$ |
| Compression Strength–Failure | $f_m = 2.24 \text{ N/mm}^2$ |
| Elastic Modulus | $E = 20,500 \text{ kg/cm}^2$ |
| Average Specific Weight | $w = 1750 \text{ kg/m}^3$ |
| Poisson Modulus | $\nu = 0.24$ |

Therefore, the mechanical characteristics of the materials used for building modelling are summarized in Tables 2 and 3. Such resistance characteristics values are divided by the Confidence Factor, which is 1.20 and 1.35 in the case of LC2 and LC1, respectively.

Table 2. Masonry with regular ashlar of soft stone (tuff)-FC = 1.20.

| Characteristics | Value |
|--|-------------------------------|
| Medium compressive strength | $f_m = 224 \text{ N/cm}^2$ |
| Medium shear strength | $\tau_0 = 6.0 \text{ N/cm}^2$ |
| Normal modulus of elasticity | $E = 2090 \text{ MPa}$ |
| Tangential modulus of elasticity | $G = 667 \text{ MPa}$ |
| Partial safety coefficient for compressive strength of masonry | $\gamma_M = 3$ |

Table 3. Split stone masonry with good texture-FC = 1.35.

| Characteristics | Value |
|--|-------------------------------|
| Medium compressive strength | $f_m = 260 \text{ N/cm}^2$ |
| Medium shear strength | $\tau_0 = 5.6 \text{ N/cm}^2$ |
| Normal modulus of elasticity | $E = 1740 \text{ MPa}$ |
| Tangential modulus of elasticity | $G = 580 \text{ MPa}$ |
| Partial safety coefficient for compressive strength of masonry | $\gamma_M = 3$ |

2.2. Geotechnical Aspects

Based on the HVSR type seismic tests performed, the investigated soil is classifiable, according to §3.2.2 of NTC 18, as category C, that corresponds to “Deposits of medium thickened coarse-grained soils or medium-consistent fine-grained soils with substrate depths greater

than 30 m, characterized by an improvement in mechanical properties with depth and equivalent speed values between 180 m/s and 360 m/s”.

Topographic conditions are classifiable, according to §3.2.3 of NTC 18, as category T1, which is defined as “flat surfaces, slopes, and isolated reliefs with medium inclination $i \leq 15^\circ$ ”, whose topographic amplification coefficient S is equal to 1.

3. Static and Seismic Analyses

3.1. The Considered Limit States

The seismic analysis is conducted using as references the Update of the “Technical Standards for Constructions” and the related Circular “Instructions for the application of the New Technical Standards for Constructions”. In particular, the indications contained in Chapters 7 (“Design for seismic actions”) and 8 (“Existing buildings”) of both regulatory references have been followed and applied [19,20].

To assess seismic safety, the building under analysis was considered within the class of use III, which corresponds to constructions whose use involves significant crowding. Therefore, depending on this class of use, a nominal life of 50 years was assumed and a coefficient of use $C_u = 1.5$ was considered, so that the reference period $V_R = 50 \times 1.5 = 75$ years.

Taking into account the class of use of the building, its performance levels have been analysed including, in addition to the ultimate limit states (collapse and life safety), as well as serviceability ones (damage and operational limit states), as indicated by Chapter 8 of the Legislative Decree 17/01/2018 (NTC 18).

Table 4 reports the indicative parameters of the probability of occurrence (PVR) and return time (TR) for each limit state used for verification purposes. However, the evaluation of the building strength and ductility was conducted with reference to the Life Safety (LS) Limit State, whose elastic spectrum is shown in Figure 14.

Table 4. PVR and TR parameters for Ultimate and Serviceability limit states.

| LS | | D | | O | |
|-----|-----------|-----|----------|-----|----------|
| PVR | T_R | PVR | T_R | PVR | T_R |
| 10% | 712 years | 63% | 75 years | 81% | 45 years |

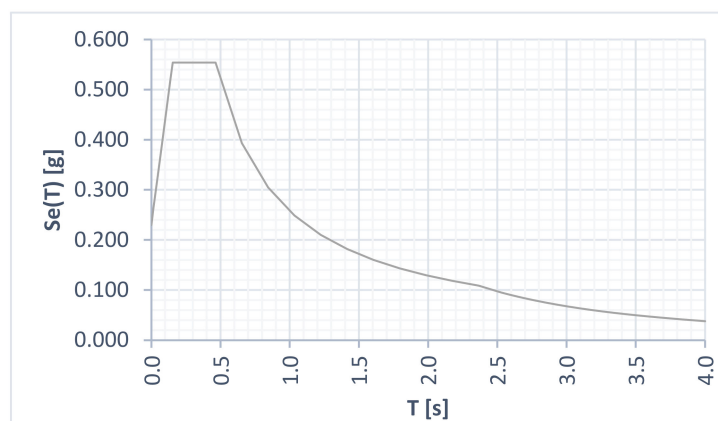


Figure 14. Elastic response spectrum at LS limit state.

3.2. FME Modelling Approach and Building Features

The numerical elaborations for the structural and seismic investigation of the building were conducted with the software delivered by the S.T.A.data company. TreMuri is a seismic and static calculation software for masonry structures according to the modern codes (NTC 2018, EC8, SIA).

The calculation program is based on the FME (Frame by Macro Element) method [21,22]. The structure is schematized through macro-elements to analyse its seismic behaviour in

detail. Specifically, a wall is discretized into two types of deformable macroelements: the first representative of masonry piers and the second corresponding to spandrels. The wall portions connecting piers and spandrels are called rigid nodes; they represent the areas of masonry less subjected to seismic damage.

3.3. Analysis of Loads

The analysis of loads is performed based on what emerged from the endoscopic and thermographic tests on the floors. The calculations carried out, therefore, consider material-specific requirements, joisted floor loads (dead loads G_{1k} , permanent loads G_{2k} and live loads Q_k), snow actions and earthquake forces, which are defined following prescriptions of NTC 18.

Therefore, once the loads have been defined, the fundamental and the seismic combinations are considered assuming the following loads values:

- G_1 : dead weight of mixed RC joists-hollow tiles floor = 4.54 kN/m^2 ;
- G_2 : dead weight of mixed ribbed RC joists-hollow tiles floor with = 5.13 kN/m^2 ;
- G_3 : dead weight of all non-structural elements = 2.30 kN/m^2 ;
- Q_{ki} : characteristic value of the i -th variable action = 3.00 kN/m^2 ;
- ψ_{0i} : combination coefficients to consider the reduced probability of concomitance of the variable actions with their respective characteristic values, chosen by the intended use of the various floors, as indicated in Table 2.5.1 of NTC 18. In this case, $\psi_0 = 0.7$ for live loads in residential environments and environments susceptible to crowding, $\psi_0 = 0.5$ for snow loads and $\psi_0 = 0$ for live loads on roofs accessible for maintenance only.

With regards to the values of the seismic combination, the following ones are assumed:

- $\psi_2 = 0.6$ for live loads in environments susceptible to crowding, such as schools;
- $\psi_2 = 0.3$ for live loads in residential environments;
- $\psi_2 = 0$ for snow loads and attics.

For the load combinations in linear analyses, actions are applied to the structure considering the possible combinations of verse and eccentricity.

To define, instead, the load combinations in nonlinear static analyses, the elementary load conditions that could happen simultaneously, as well as the presence of the accidental eccentricity (which is equal to 5% of the size of the building side orthogonal to the earthquake direction considered), were cumulated in different ways with the standard safety factors, obtaining 24 load combinations.

3.4. Structure Modelling and Analysis Checks

3.4.1. Premise

The structural modelling is performed by applying the numerical software TreMuri version 13.2.0.0. The aim is to adequately represent the distribution of mass and actual stiffness of the building.

The structural elements included in the geometric model are all the wall vestments reputed to be able to withstand vertical and horizontal actions. For masonry, the Turnšek–Cacovic model was used.

The presence of door and window compartments is appropriately considered in size and location. A three-dimensional view of the building modelling is depicted in Figure 15. A view of the 3D macro-elements model of the school is instead reported in Figure 16.

On the structure under study, the following types of analysis are chosen and applied:

- a linear static analysis for static checks under gravity loads;
- a linear kinematic analysis to verify local failure mechanisms;
- a non-linear static (pushover) analysis for global seismic analysis.

Before performing all the above-mentioned analyses, a modal investigation was performed in order to obtain the mode shapes of the structure. In Table 5, the results are reported.

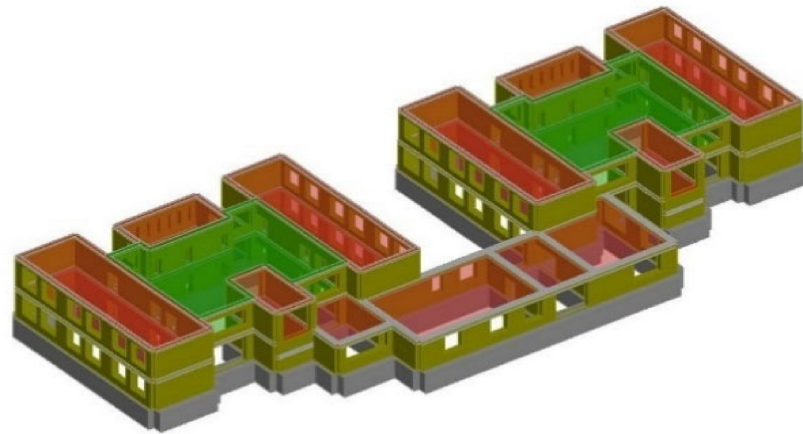


Figure 15. View of the 3Muri model of the school building.

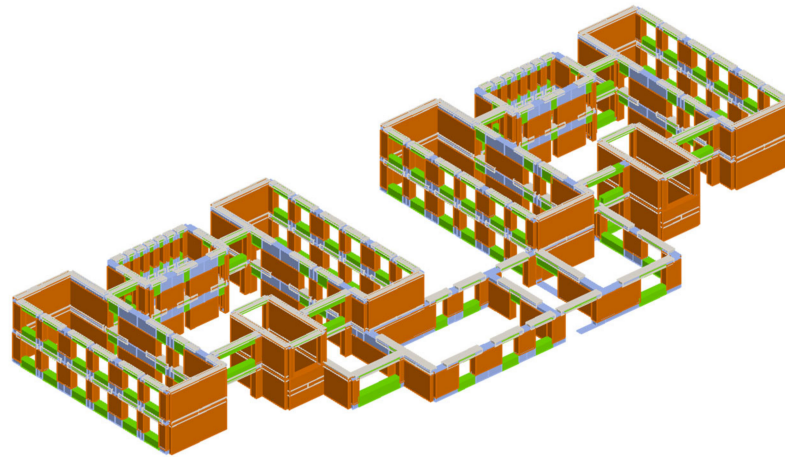


Figure 16. 3D view of the macro-elements model of the school building.

Table 5. Mode shapes and vibration periods of the school building.

| Modo | T [s] | mx [kg] | Mx [%] | my [kg] | My [%] | mz [kg] | Mz [%] |
|------|---------|-----------|--------|-----------|--------|---------|--------|
| 1 | 0.23777 | 2.583.456 | 86.02 | 35 | 0.00 | 0 | 0.00 |
| 2 | 0.21297 | 11 | 0.00 | 48.636 | 1.62 | 0 | 0.00 |
| 3 | 0.19674 | 13.682 | 0.46 | 10.722 | 0.36 | 1 | 0.00 |
| 4 | 0.18234 | 26 | 0.00 | 2.368.538 | 78.86 | 30 | 0.00 |
| 5 | 0.17285 | 4.341 | 0.14 | 160.090 | 5.33 | 21 | 0.00 |
| 6 | 0.16274 | 3.423 | 0.11 | 54.892 | 1.83 | 65 | 0.00 |
| 7 | 0.11515 | 385.897 | 12.85 | 176 | 0.01 | 20 | 0.00 |
| 8 | 0.09681 | 199 | 0.01 | 3.727 | 0.12 | 1 | 0.00 |
| 9 | 0.08988 | 4.139 | 0.14 | 311 | 0.01 | 7 | 0.00 |
| 10 | 0.08473 | 10 | 0.00 | 341.891 | 11.38 | 199 | 0.01 |
| 11 | 0.08143 | 1.103 | 0.04 | 1.073 | 0.04 | 256 | 0.01 |
| 12 | 0.07834 | 429 | 0.01 | 5.102 | 0.17 | 111 | 0.00 |
| 13 | 0.06650 | 5 | 0.00 | 0 | 0.00 | 19.307 | 0.64 |
| 14 | 0.06645 | 2 | 0.00 | 1 | 0.00 | 441.342 | 14.69 |
| 15 | 0.06633 | 3 | 0.00 | 1 | 0.00 | 143.078 | 4.76 |
| 16 | 0.06617 | 5 | 0.00 | 119 | 0.00 | 259.135 | 8.63 |
| 17 | 0.06485 | 59 | 0.00 | 5 | 0.00 | 43.873 | 1.46 |
| 18 | 0.06412 | 1 | 0.00 | 0 | 0.00 | 20 | 0.00 |
| 19 | 0.06412 | 0 | 0.00 | 0 | 0.00 | 225.470 | 7.51 |
| 20 | 0.06398 | 0 | 0.00 | 1 | 0.00 | 110.970 | 3.69 |

The first vibration mode is in the x direction with a participating mass of about 86.02%, while in the orthogonal direction, the first significant shape mode is the number 4 with a participating mass of about 78.86%. The deformed shape in the two main directions are represented in Figures 17 and 18.

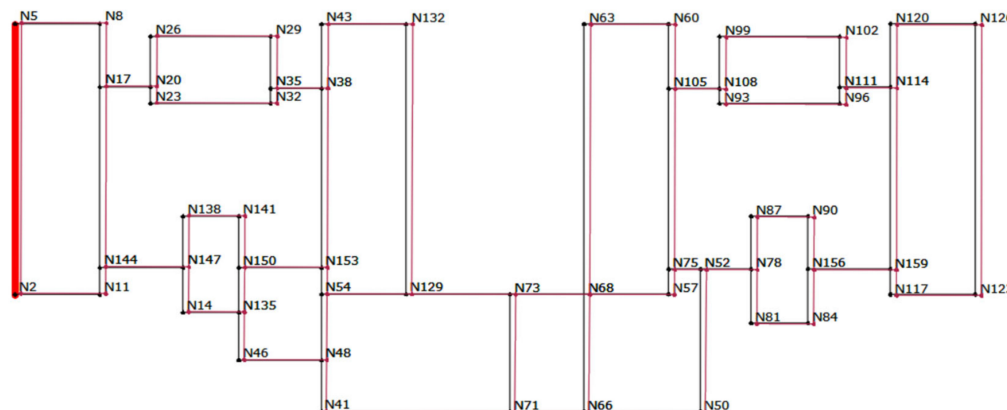


Figure 17. Deformed shape of the original building in the x direction.

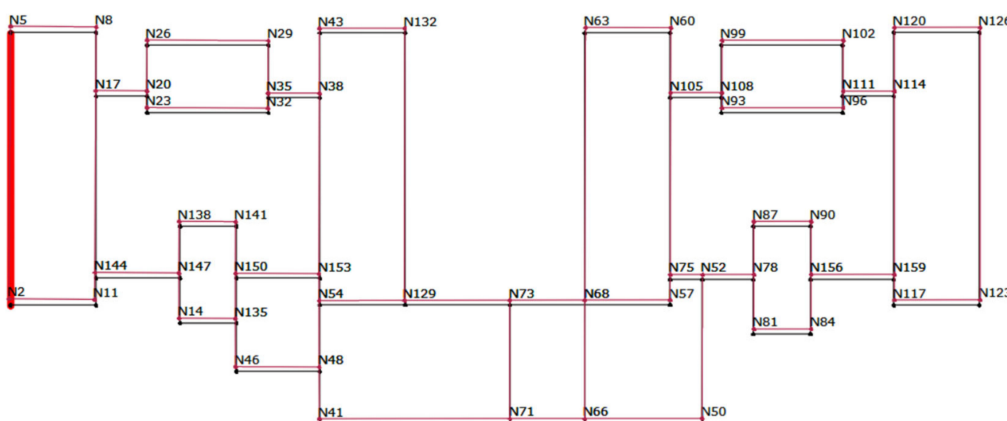


Figure 18. Deformed shape of the original building in the y direction.

According to the current Italian technical code, the pushover analysis is “applicable to masonry buildings as described in §7.3.4.2, with the possibility of extend the method to structures having in the direction considered a participating mass not less than 60%”.

3.4.2. Static Checks

Static checks are performed following paragraphs 4.5.4 and 4.5.6. of NTC 18.

To this end, the slenderness of masonry is considered, which is defined as the ratio h_0/t , where:

- h_0 = free breaking length of the wall, equal to $\rho \cdot h$;
- t = wall thickness;
- h = internal floor height;
- ρ = lateral constraint factor [Tab. 4.5.IV of NTC 18].

The verification is satisfied if the following inequality is verified:

$$h_0/t \leq 20 \quad (1)$$

In addition, a simplified check method towards stress induced by vertical loads is considered. In this case, for masonry walls, the acting vertical load value and the resistant vertical load are compared to each other. This assessment examines the values of slenderness and eccentricity [§4.5.6 of NTC 18].

The verification is fulfilled if the following inequality is verified:

$$N_d \leq N_r \quad (2)$$

where

- N_d : applied vertical load;
- N_r : resistant vertical load, equal to $\Phi * f_d * A$;
- A : area of the horizontal section of the wall without openings;
- f_d : masonry calculation stress;
- Φ : coefficient of reduction of the wall resistance.

The value of Φ and, therefore, of the normal resistant stress, can be calculated only if the checks about slenderness and eccentricity of the loads are satisfied.

In particular, regarding eccentricities, the following conditions must always be verified:

$$e_1/t \leq 0.33 \quad (3)$$

$$e_2/t \leq 0.33 \quad (4)$$

Being t the thickness of the wall, with e_1 and e_2 calculated as follows:

$$e_1 = |e_s| + e_a; \quad e_2 = \left| \frac{e_1}{2} \right| + |e_v| \quad (5)$$

where:

- e_s : total eccentricity of vertical loads;
- e_a : eccentricity due to execution tolerances, equal to $h/200$, with h = internal floor height;
- e_v : eccentricity due to horizontal actions applied in the direction normal to the masonry plane, equal to M_v/N .

The checks were conducted in the three main sections (lower, central and upper) of each masonry panel of the structure walls.

From the analysis results, it can be seen that several ground story panels do not satisfy the static checks. A three-dimensional view of the structure 3Muri model subjected to vertical loads is illustrated in Figure 19, where the masonry panels unable to overpass the static verification at the Ultimate Limit State are shown with pink colour.

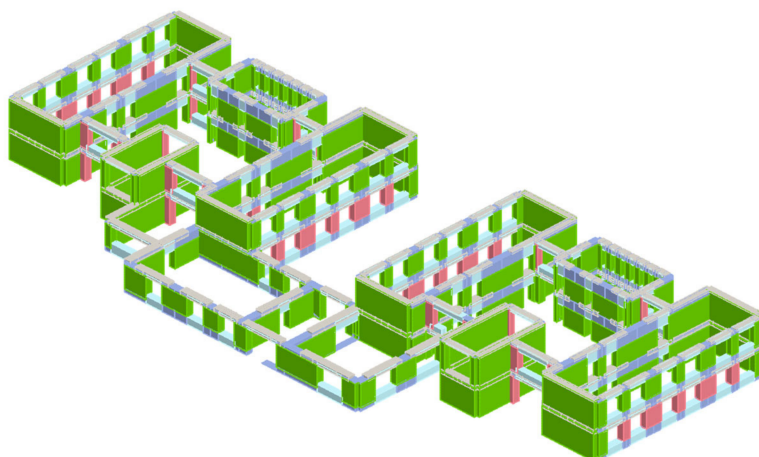


Figure 19. Static verification mapping at the Ultimate Limit State.

3.4.3. Verification of Local Mechanisms

In existing masonry buildings, partial collapses often occur due to seismic actions usually due to loss of the balance of wall portions. These mechanisms, according to the methods described below, take place if a specific monolithic nature of the wall is guaranteed, such as to prevent punctual collapses due to the disintegration of assembled blocks.

The checks regarding local mechanisms can be conducted through the limit analysis of equilibrium, according to the kinematic approach, which is based on the choice of the collapse mechanism and the evaluation of the horizontal action activating this kinematics.

For each possible local mechanism considered as significant for the building, the method is divided into the following steps:

- Transformation of a part of the construction into a labile system (kinematic chain) through identifying rigid bodies, defined by hypothetical fracture planes able to rotate or slide on each other;
- Evaluation of the horizontal multiplier of loads α_0 , which involves the activation of the mechanism using the principle of virtual works;
- Identification of the spectral seismic acceleration of activation a_z starting from the horizontal multiplier of the loads α_0 .

The coefficient α_0 is obtained by applying the following forces to the rigid blocks that make up the kinematic chain:

- The blocks' weight applied in the centre of gravity;
- Vertical loads due to dead weights and live loads of floors and weight of non-structural wall elements;
- Horizontal forces proportional to the vertical loads carried, if not effectively transmitted to the building;
- External forces transmitted by connecting elements, such as chains;
- Any internal forces related to the meshing between the wall ashlars.

It is important to note that herein, given the presence of the inter-storey ring beams, the verification of the simple overturning mechanisms is always satisfied for each wall analysed. As a result, the parameter α is always greater than 1.

3.4.4. Global Seismic Checks

For the global seismic analysis, the required checks compare the capacity curve for the different conditions envisaged and the demand one needed by the current legislation standard NTC 18.

The capacity curve is identified through the base shear-displacement diagram. According to the requirements of the legislation, at least two distributions of inertia forces must be considered, one falling within the principal distributions (Group 1) and the other in the secondary distributions (Group 2) illustrated below:

- Distribution proportional to the static forces (Group 1);
- Uniform distribution of forces, which is derived from a uniform distribution of accelerations over the height of the construction (Group 2).

The analysis, performed in displacement control monitoring a point called the "control node", proceeds with calculating the forces distribution that generates the required displacement value. The analysis is continued until the decay of the shear to 80% from its peak value occurs. Thus, the value of the maximum displacement at the base of the building generated by that distribution of forces is calculated. This displacement value is the ultimate value attained by the building.

The legislation requires tracking a bi-linear capacity curve of an equivalent system (SDOF). The tracking of this curve must take place with a straight line that, passing through the origin, intersects the curve of the real system at 70% of the peak value; the second line is instead parallel to the axis of displacements such as to generate the equivalence of the areas between the diagrams of the real system and the equivalent one.

The determination of the equivalent system curve allows determining the period to obtain the maximum displacement required by the earthquake, according to the spectra reported in the standard code.

Based on the type of building and the design choices that are considered most suitable, it is possible to decide the seismic load condition to be examined as follows:

- Seismic load: identifies which of the two types of distributions (proportional to either the masses or the first mode) should be considered;
- Direction: identifies the direction (X or Y of the global system) along which the structure is loaded by the seismic load.

To identify the most severe seismic load combination, it is decided to perform the analyses considering the two load types, the two directions of the earthquake and any accidental eccentricities.

In Figure 20, the results of the 24 pushover analyses performed in the x and y directions, with seismic load proportional to the masses and the first vibration mode applied with and without eccentricities are reported.

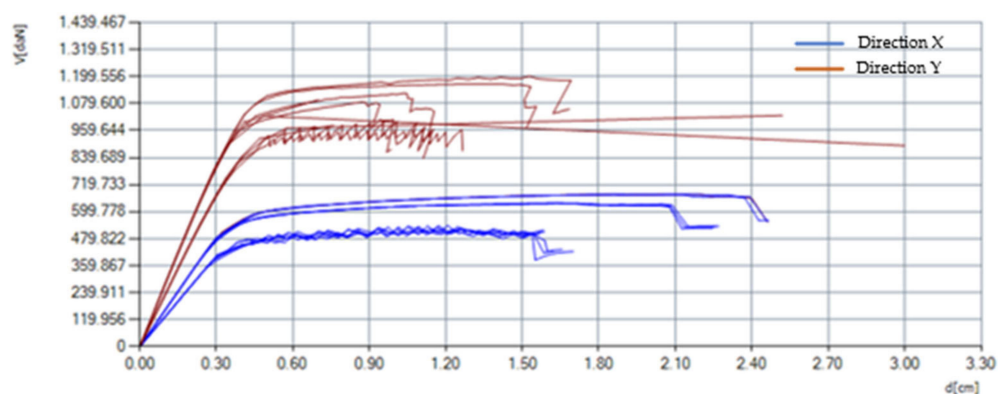


Figure 20. Results of pushover analyses.

The pushover analyses identify the lowest seismic risk safety factors in directions x and y, which are equal to 0.592 and 0.622, respectively, so as to show the inadequacy of the school building to withstand the design seismic actions at the Life Safety Limit State. From these analyses, it is also possible to identify the wall panels in the worst conditions under earthquake and to associate the mechanism type inducing the crisis of the masonry parts.

In Figure 21, the damages of masonry panels in the worst analysis case in direction x are shown. From this analysis, it is apparent that wall panels exhibit some collapses due to compression-bending and shear mechanisms at the top storey.

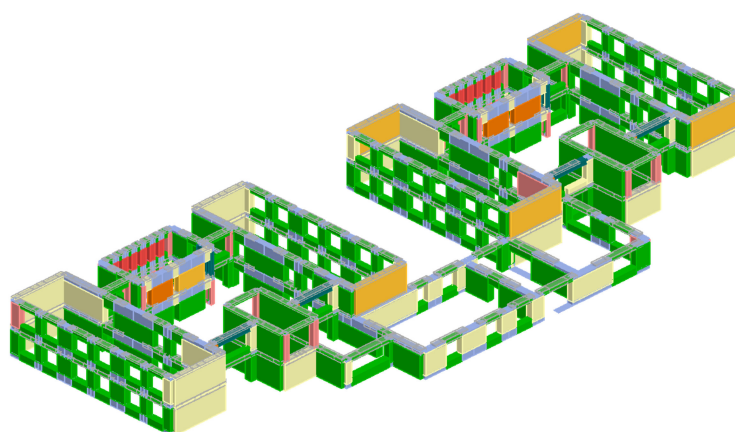


Figure 21. Damage state of the building in the worst analysis case in longitudinal (X) direction. Legend: green and grey: no damage; dark green: incipient plasticity; pink: compressive-bending plastic; magenta: serious crisis; yellow: shear plastic; orange: incipient shear failure; dark orange: shear failure.

With regard to the evaluation of ductility, the corresponding factor μ is calculated through the following expression:

$$\mu = \frac{d_u}{d_y} - 1 \quad (6)$$

which gives rise to a factor equal to 2.08 for the building in its original state.

3.4.5. Verification of Foundations

The verification of the foundation system is mandatory, as stated by §8.3 of NTC 18, only if global instability phenomena occur or if one of the following conditions is met:

- In the construction, substantial instability is attributed to subsidence of the foundations or instability of the same nature occurred in the past;
- The phenomena of overturning and/or sliding of the building are possible due to unfavourable morphological conditions, changes made to the ground profile near the foundations and design seismic actions;
- Liquefaction phenomena of the foundation soil due to the design seismic activities are possible.

In our case, due to the inexistence of the above conditions, it was not necessary to deepen the characteristics of the foundation system and proceed, therefore, with the related checks.

3.4.6. Seismic Risk Class

This section reports the assessment of the seismic risk class obtained following the indications contained in the Italian Guidelines [23], that allow attributing to buildings, using either a conventional or a simplified method, a specific Seismic Risk Class, from A+ (lowest risk) to G (highest risk), through a single parameter accounting for both safety and economic aspects.

Concerning the conventional method for determining the risk class, the following two parameters are determined:

- Economic Parameter: PAM Class (Expected Average Annual Loss): cost of repairing the damage caused by seismic events that will occur during the life of the building, distributed annually and expressed as a percentage of the reconstruction cost.
- Safety Parameter: IS-V Class (Safety Index): the ratio between the peak acceleration on the ground that determines the achievement of the Life Safeguard Limit State and that envisaged, on-site, for a new building.

In Table 6, the ranges of values for the different seismic risk classes of the two parameters are reported.

Table 6. Ranges for each seismic class.

| Safety Index | IS-V Class |
|------------------------------|--------------|
| $100\% < IS-V$ | A_{IS-V}^+ |
| $80\% \leq IS-V < 100\%$ | A_{IS-V} |
| $60\% \leq IS-V < 80\%$ | B_{IS-V} |
| $45\% \leq IS-V < 60\%$ | C_{IS-V} |
| $30\% \leq IS-V < 45\%$ | D_{IS-V} |
| $15\% \leq IS-V < 30\%$ | E_{IS-V} |
| $IS-V \leq 15\%$ | F_{IS-V} |
| Expected Average Annual Loss | PAM Class |
| $PAM \leq 0.50\%$ | A_{PAM}^+ |
| $0.50\% < PAM \leq 1.0\%$ | A_{PAM} |
| $1.0\% < PAM \leq 1.5\%$ | B_{PAM} |
| $1.5\% < PAM \leq 2.5\%$ | C_{PAM} |
| $2.5\% < PAM \leq 3.5\%$ | D_{PAM} |
| $3.5\% < PAM \leq 4.5\%$ | E_{PAM} |
| $4.5\% < PAM \leq 7.5\%$ | F_{PAM} |
| $7.5\% \leq PAM$ | G_{PAM} |

The results of the seismic classification for the school building herein examined provide a seismic risk class C, as reported in Figure 22.

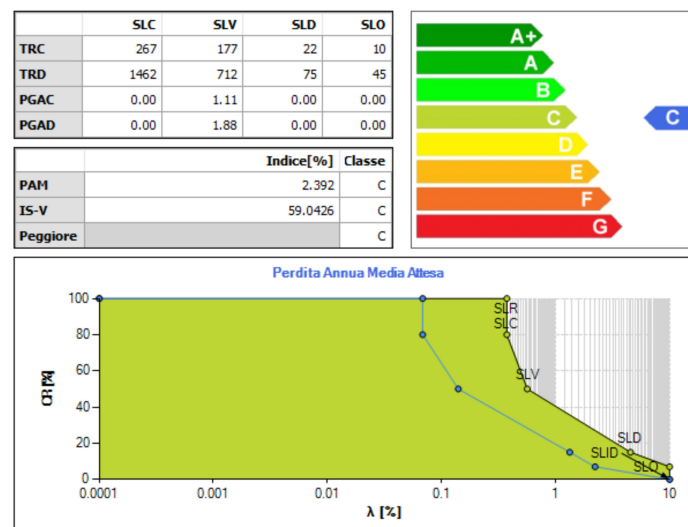


Figure 22. Seismic classification of the school building in the current state.

For assessment of seismic risk class referred to each limit state, the capacity and demand of both return period (T_R) and peak ground acceleration (PGA) have been considered. In particular, the ratio between the PGAs gives rise to the IS-V index. Contrary, the ratio between the return periods provides, through a specific formula, the PAM index.

In the case under study, a seismic risk class equal to C has been obtained. This means that IS-V is included in the range between 45% and 60%, whereas the PAM is in the range between 1.5% and 2.5%.

4. FRP and FRCM-Based Retrofit Interventions

4.1. Selection of the Control Node

To solve, in whole or in part, the structural vulnerabilities found through the analysis of the current state building, it is possible to define alternative intervention strategies to increase the resistant capacity of the structure.

The solutions proposed for the intervention concern the use of FRP/FRCM systems to reinforce the masonry walls exhibiting failure from pushover analyses.

In the case of FRP-based technique, this technique was applied with bands arranged in three layers, each with thickness of 0.165 mm, having width of 30 cm and pitch of 50 cm. On the other hand, when the FRCM technique was considered, a single layer with thickness of 0.06 mm was placed on both sides of walls.

The pushover analysis was performed by choosing, as indicated by the standard code, a control node close to the barycentric point of the last floor (node 130 in Figure 23). However, given the in-plan and in-elevation irregular conformation of the building, nodes 142 and 127 were also chosen as further control nodes to evaluate the variation of the analysis results and, therefore, to select the most reliable node for subsequent evaluations.

The pushover analysis results in terms of seismic risk class attribution considering the above-selected control nodes are illustrated in Table 7.

Table 7. Results of seismic risk class analysis considering different control nodes.

| Reference Node | α_{SLV} | PAM | IS-V | Class |
|----------------|-----------------|------|-------|-------|
| Node 127 | X: 0.59 Y: 0.62 | 2.39 | 59.04 | C |
| Node 142 | X: 0.56 Y: 0.70 | 2.13 | 56.38 | C |
| Node 130 | X: 0.58 Y: 0.70 | 2.39 | 57.98 | C |

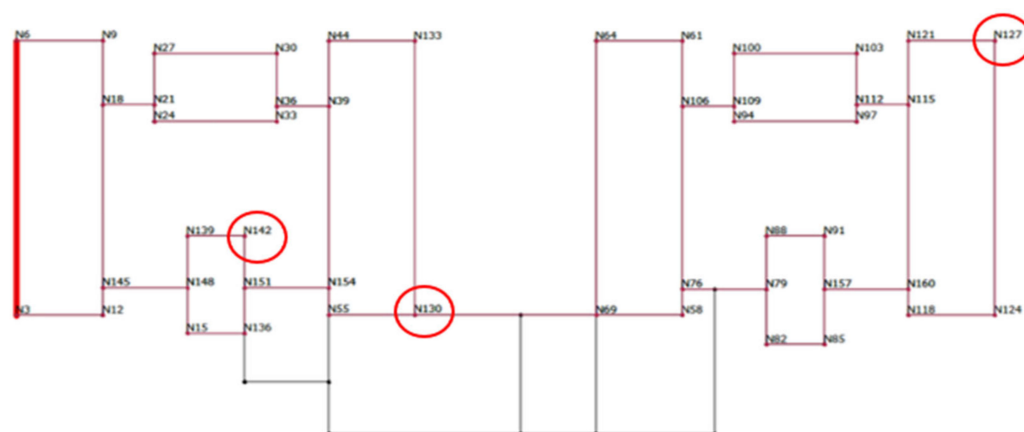


Figure 23. The control nodes monitored in pushover analyses (Red circle show control nodes).

Based on these results, the node chosen for comparing the seismic performances of the building retrofitted with the two selected systems (FRP and FRCM) was that with label 127.

The total number of masonry walls subjected to retrofit interventions are 8 in direction x and 15 in direction y, as depicted in Figure 24.

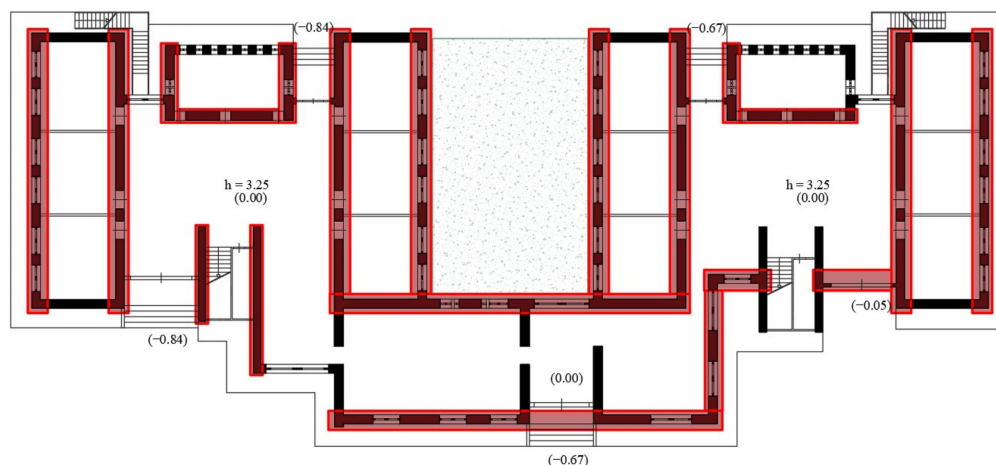


Figure 24. A graphic representation of strengthened masonry walls.

The design of the above-mentioned systems and the analysis results deriving from retrofit interventions are reported in the sections below.

4.2. Retrofit with FRP Systems

FRP, an acronym for Fibre-Reinforced Polymers or Fibre-Reinforced Plastic, defines fibre-reinforced materials in a polymer matrix. The reinforcement can be made up of fibres with different chemico-physical characteristics, such as carbon, glass, or aramid, while the matrix is of organic type. Products obtained by pultrusion are also included in the FRP category [1].

The system, which can be impregnated on-site or pre-impregnated (FRP preformed), consists of three layers: matrix, fabric and adhesive.

These composites are characterized by high tearing resistance, excellent resistance in a humid environment and excellent mechanical performances [24]. The matrix, in fact, guarantees a high load distribution between the fibres and high adhesion performance to the support [25].

Despite the many advantages associated with their use, it is also required to remember some disadvantages including low shear resistance, poor resistance to high temperatures and poor breathability of the supports. In the case under study, an FRP system composed

of carbon fibre fabric and an epoxy resin matrix was chosen as retrofit intervention. This system is applied with bands arranged in three layers, each with thickness of 0.165 mm, with width of 30 cm and pitch of 50 cm, as depicted in Figure 25. Young's modulus and nominal ultimate strain of carbon fibres are equal to 229,000 MPa and 1.58%, respectively.

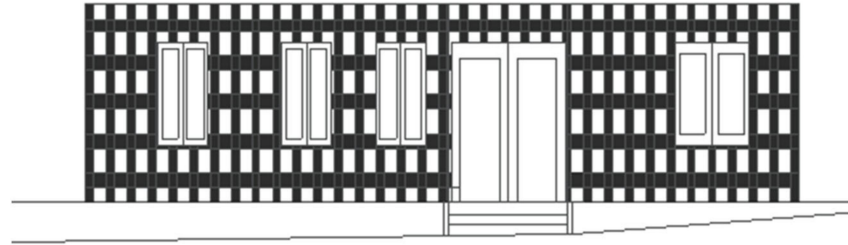


Figure 25. A graphic representation of a school masonry wall retrofitted with an FRP system.

The analysis results on the retrofitted building in terms of the most unfavourable pushover curves in directions X and Y are provided in Figures 26 and 27, respectively. It was found that in this first strengthened model, the ductility factor assumes a value equal to 2.36. Moreover, the minimum seismic risk safety factors assume values of 0.97 (analysis n. 9 with uniform load distribution and eccentricity of -137.07 cm) and 0.92 (analysis n. 21 with uniform load distribution and eccentricity of 340.05 cm) in directions x and y, respectively. The results obtained demonstrate the reliability of the proposed system, which allows to increase the seismic safety factors of the inspected buildings of at least 0.1 in both directions, so as to attain the seismic upgrading of the structure.

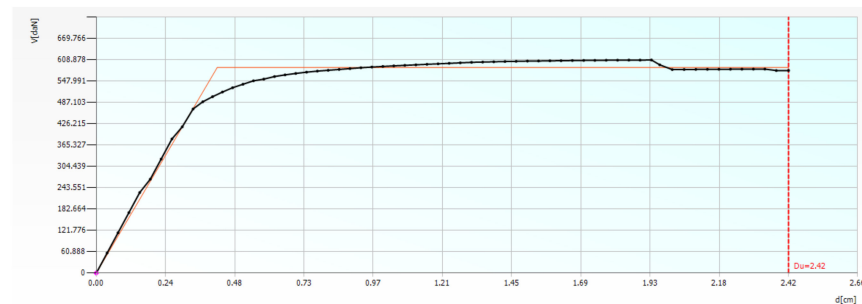


Figure 26. Worst pushover curve in direction x on the building retrofitted with an FRP system (Black curve is the pushover, red one corresponds to bilinear equivalent).

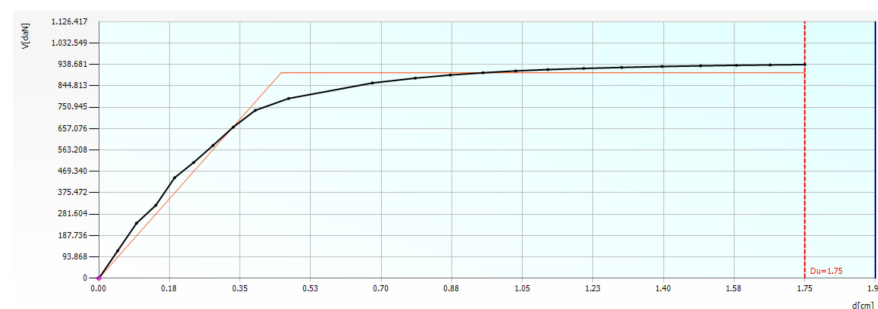


Figure 27. Worst pushover curve in direction y on the building retrofitted with an FRP system.

The seismic risk classification of the building after intervention with calculation of both PAM and IS-V parameters provide a class A, as presented in Figure 28.

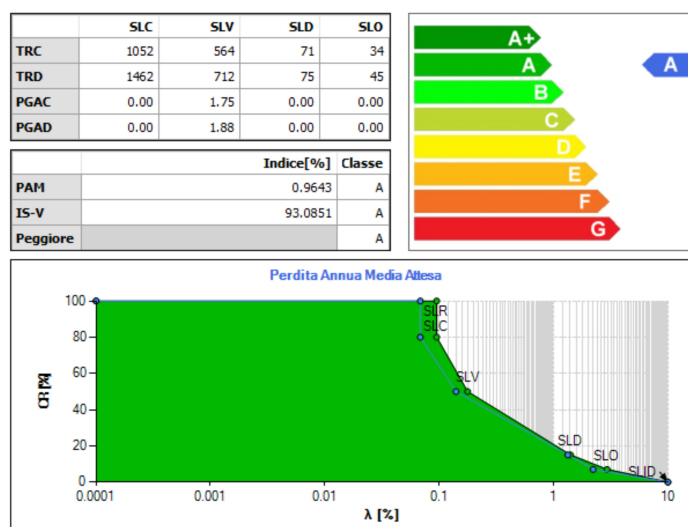


Figure 28. Seismic risk classification of the building retrofitted with an FRP system.

Additionally, in this case, before conducting the pushover analyses, the modal one was performed in order to obtain the mode shapes of the structure. In Table 8, the results are reported.

Table 8. Mode shapes and vibration periods of the school building with the FRP system.

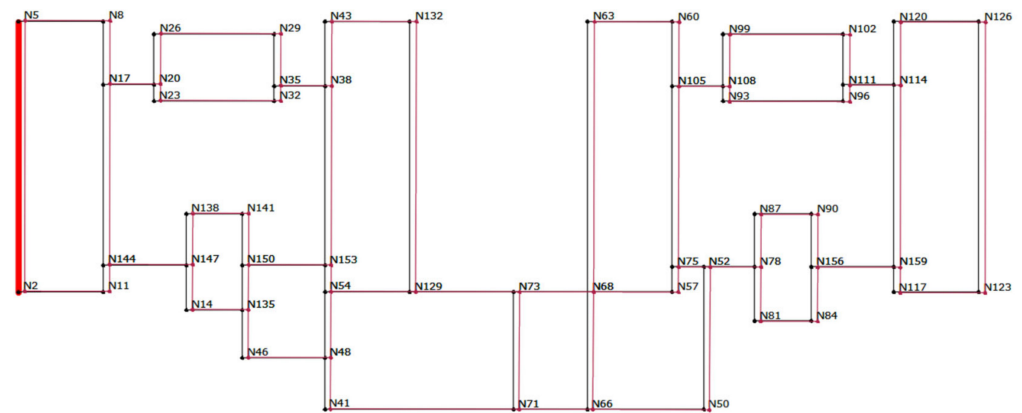
| Modo | T [s] | mx [kg] | Mx [%] | my [kg] | My [%] | mz [kg] | Mz [%] |
|------|---------|-----------|--------|-----------|--------|---------|--------|
| 1 | 0.23339 | 2.313.009 | 86.02 | 23 | 0.00 | 0 | 0.00 |
| 2 | 0.21123 | 63 | 0.00 | 42.718 | 1.59 | 0 | 0.00 |
| 3 | 0.19776 | 3.904 | 0.15 | 7.884 | 0.29 | 0 | 0.00 |
| 4 | 0.18112 | 18 | 0.00 | 1.948.996 | 72.49 | 33 | 0.00 |
| 5 | 0.17515 | 4.760 | 0.18 | 210.666 | 7.83 | 30 | 0.00 |
| 6 | 0.16552 | 2.679 | 0.10 | 108.928 | 4.05 | 43 | 0.00 |
| 7 | 0.11311 | 346.026 | 12.87 | 148 | 0.01 | 32 | 0.00 |
| 8 | 0.09591 | 380 | 0.01 | 6.998 | 0.26 | 0 | 0.00 |
| 9 | 0.09344 | 114 | 0.00 | 16.351 | 0.61 | 4 | 0.00 |
| 10 | 0.09304 | 14 | 0.00 | 28.048 | 1.04 | 33 | 0.00 |
| 11 | 0.08965 | 649 | 0.02 | 22 | 0.00 | 14 | 0.00 |
| 12 | 0.08814 | 42 | 0.00 | 583 | 0.02 | 3 | 0.00 |
| 13 | 0.08692 | 2.695 | 0.10 | 86 | 0.00 | 30 | 0.00 |
| 14 | 0.08180 | 0 | 0.00 | 288.298 | 10.72 | 268 | 0.01 |
| 15 | 0.07945 | 809 | 0.03 | 2.291 | 0.09 | 112 | 0.00 |
| 16 | 0.07678 | 479 | 0.02 | 11.533 | 0.43 | 207 | 0.01 |
| 17 | 0.07015 | 3.472 | 0.13 | 64 | 0.00 | 27 | 0.00 |
| 18 | 0.06659 | 253 | 0.01 | 0 | 0.00 | 264 | 0.01 |
| 19 | 0.06638 | 4 | 0.00 | 3.525 | 0.13 | 46.180 | 1.72 |
| 20 | 0.06609 | 154 | 0.01 | 13 | 0.00 | 269 | 0.01 |

The first vibration mode is in the x direction with a participating mass of about 86.02% (the same as that of the unreinforced model), while in the orthogonal direction, the first significant shape mode is number 4 with a participating mass of about 72.49%. The deformed shape in the two main directions are represented in Figures 29 and 30.

4.3. Retrofit with FRCM Systems

FRCM systems, namely, Fibre-Reinforced Cementitious Matrix systems, are used to reinforce both externally and internally existing masonry structures. Unlike FRPs, the matrix of FRCM systems is exclusively inorganic and, therefore, based on a mortar made of lime or cement. Reinforcement consists of a grid of monodirectional elements made of

different materials, such as high-strength steel, aramid, basalt, carbon, polyparaphenylenebenzobisoxazole (PBO) and alkali-resistant glass (AR) [26].



After calculation of both PAM and IS-V parameters, a class B (instead of class A with FRP system) dictated by PAM is achieved for the seismically upgraded building.

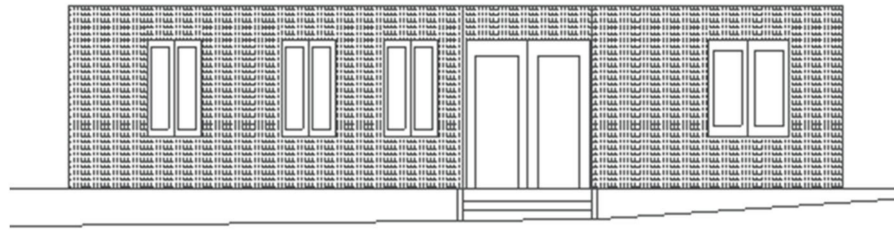


Figure 31. A graphic representation of a school masonry wall retrofitted by an FRCM system.

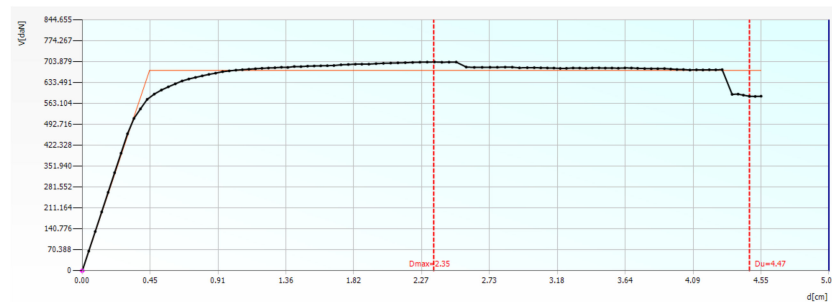


Figure 32. Worst pushover curve in direction x on the building retrofitted with an FRCM system.

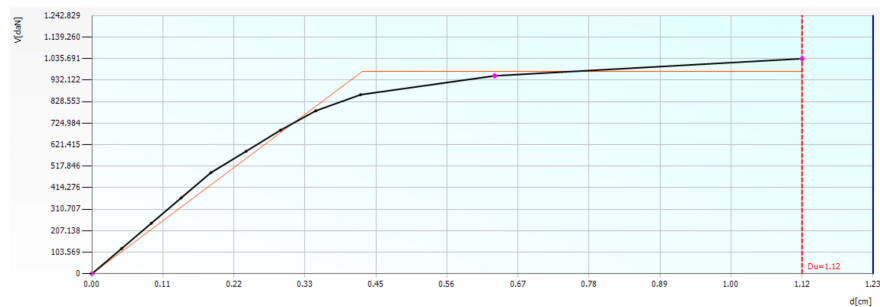


Figure 33. Worst pushover curve in direction y on the building retrofitted with an FRCM system.

The building model reinforced with FRCM system shows a ductility factor equal to 0.5.

In conclusion, Table 9 illustrates the results of the modal analysis on the last model, the one reinforced with an FRCM system.

Table 9. Mode shapes and vibration periods of the school building with an FRCM system.

| Modo | T [s] | mx [kg] | Mx [%] | my [kg] | My [%] | mz [kg] | Mz [%] |
|------|---------|-----------|--------|-----------|--------|---------|--------|
| 1 | 0.23392 | 2.336.254 | 86.10 | 50 | 0.00 | 0 | 0.00 |
| 2 | 0.21139 | 450 | 0.02 | 40.820 | 1.50 | 1 | 0.00 |
| 3 | 0.19769 | 3.639 | 0.13 | 7.468 | 0.28 | 0 | 0.00 |
| 4 | 0.18131 | 3 | 0.00 | 2.009.003 | 74.04 | 47 | 0.00 |
| 5 | 0.17545 | 5.007 | 0.18 | 173.836 | 6.41 | 30 | 0.00 |
| 6 | 0.16564 | 2.619 | 0.10 | 112.021 | 4.13 | 45 | 0.00 |
| 7 | 0.11356 | 346.688 | 12.78 | 128 | 0.00 | 24 | 0.00 |
| 8 | 0.09621 | 765 | 0.03 | 6.225 | 0.23 | 0 | 0.00 |
| 9 | 0.09348 | 71 | 0.00 | 19.596 | 0.72 | 8 | 0.00 |
| 10 | 0.09307 | 7 | 0.00 | 28.558 | 1.05 | 30 | 0.00 |
| 11 | 0.08980 | 840 | 0.03 | 151 | 0.01 | 16 | 0.00 |
| 12 | 0.08813 | 7 | 0.00 | 186 | 0.01 | 7 | 0.00 |
| 13 | 0.08701 | 2.612 | 0.10 | 208 | 0.01 | 11 | 0.00 |

Table 9. Cont.

| Modo | T [s] | mx [kg] | Mx [%] | my [kg] | My [%] | mz [kg] | Mz [%] |
|------|---------|---------|--------|---------|--------|---------|--------|
| 14 | 0.08192 | 3 | 0.00 | 285.154 | 10.51 | 477 | 0.02 |
| 15 | 0.07961 | 952 | 0.04 | 3.694 | 0.14 | 49 | 0.00 |
| 16 | 0.07686 | 365 | 0.01 | 12.419 | 0.46 | 157 | 0.01 |
| 17 | 0.07012 | 3.488 | 0.13 | 57 | 0.00 | 25 | 0.00 |
| 18 | 0.06667 | 249 | 0.01 | 0 | 0.00 | 12.010 | 0.44 |
| 19 | 0.06642 | 0 | 0.00 | 3.003 | 0.11 | 60.932 | 2.25 |
| 20 | 0.06616 | 117 | 0.00 | 61 | 0.00 | 3.808 | 0.14 |

In this case, the first vibration mode is in the x direction with a participating mass of about 86.10%, while in the orthogonal direction, the first significant shape mode is number 4 with a participating mass of about 74.049%. The deformed shapes in the two main directions are represented in Figures 34 and 35.

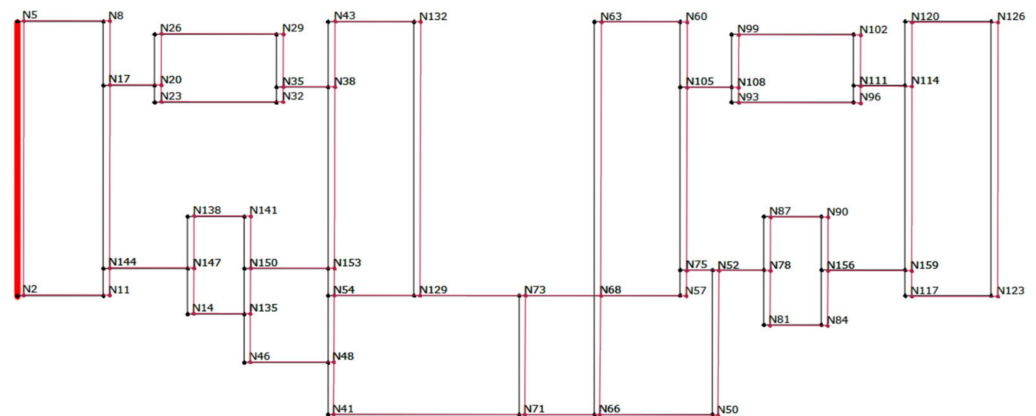


Figure 34. Deformed shape of the original building in the x direction.

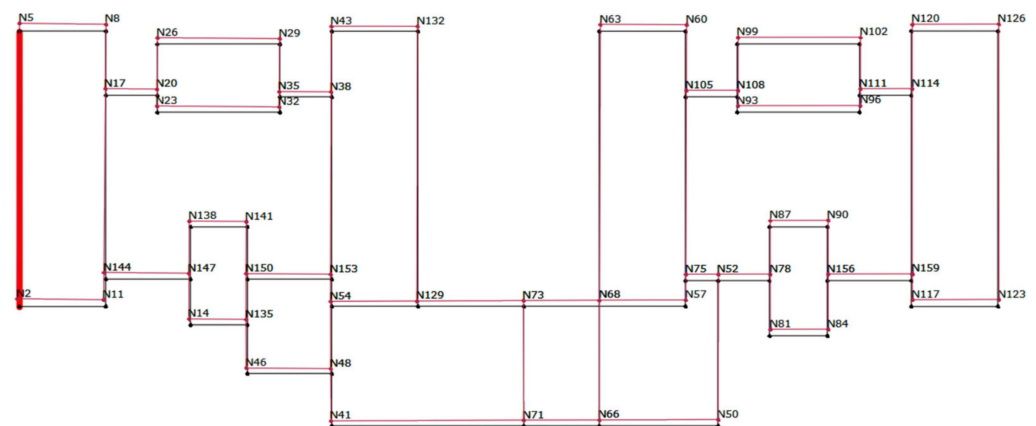


Figure 35. Deformed shape of the original building in the y direction.

4.4. Comparison of FRP and FRCM Systems

After individually evaluating the results obtained on the structure under consideration following the application of the two selected composite systems, a comparison of performances among them is drawn, as shown in Table 10.

Figure 36 shows the seismic risk classification with FRCM system.

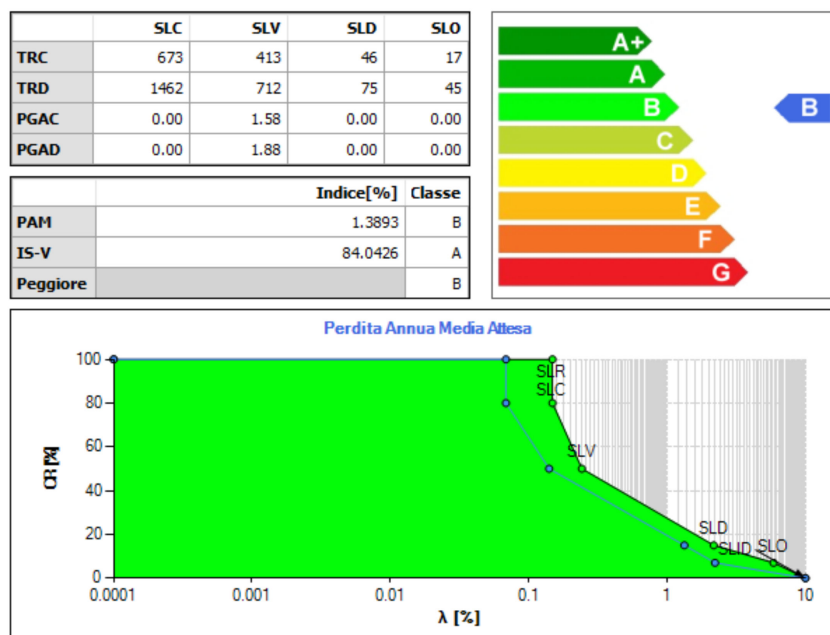


Figure 36. Seismic risk classification of the building retrofitted with an FRCM system.

Table 10. Analysis results between retrofit systems: FRP vs. FRCM.

| Type of Reinforcement | α_{SLV} | PAM | IS-V | Class |
|-----------------------|-----------------|------|-------|-------|
| FRP | X: 0.94 Y: 0.92 | 0.96 | 93.8 | A |
| FRCM | X: 0.97 Y: 0.84 | 1.38 | 84.04 | B |

Table 11 and Figure 37 show the comparison in terms of the α index between the model without any reinforcement and the one with the application of FRCM based system. It reveals the improvement of the behaviour of the structure in almost every direction.

Table 11. Comparison in terms of α between model without or with FRCM reinforcement.

| Model without Reinforcement | | | Model with FRCM | | |
|-----------------------------|-----------|----------------|----------------------------|-----------|----------------|
| $\alpha_{SLV,min} = 0.68$ | | | $\alpha_{SLV,min} = 0.843$ | | |
| Nr | Direction | α_{SLV} | Nr | Direction | α_{SLV} |
| 1 | +X | 0.967 | 1 | +X | 1.324 |
| 9 | +X; +e | 0.967 | 9 | +X; +e | 1.316 |
| 17 | +Y; +e | 0.86 | 17 | +Y; +e | 1.249 |
| 5 | +Y | 1.108 | 5 | +Y | 1.637 |
| 18 | +Y; +e | 1.564 | 18 | +Y; +e | 0.843 |
| 13 | -X; +e | 0.893 | 13 | -X; +e | 1.215 |
| 3 | -X | 0.888 | 3 | -X | 1.226 |
| 14 | -X; -e | 0.878 | 14 | -X; -e | 1.217 |
| 22 | -Y; -e | 0.68 | 22 | -Y; -e | 1.772 |
| 7 | -Y | 1.038 | 7 | -Y | 1.387 |
| 21 | -Y; +e | 0.787 | 21 | -Y; +e | 1.264 |
| 10 | +X; -e | 0.969 | 10 | +X; -e | 1.325 |

On the contrary, Table 12 and Figure 38 display, in numerical and graphical form, respectively, the improvement achieved thanks to the use of an FRP system.

Table 12. Comparison in terms of α between model without/with FRP reinforcement.

| Model without Reinforcement | | | Model with FRP | | |
|-----------------------------|-----------|----------------|----------------------------|-----------|----------------|
| $\alpha_{SLV,min} = 0.68$ | | | $\alpha_{SLV,min} = 0.843$ | | |
| Nr | Direction | α_{SLV} | Nr | Direction | α_{SLV} |
| 1 | +X | 0.967 | 1 | +X | 0.954 |
| 9 | +X; +e | 0.967 | 9 | +X; +e | 0.941 |
| 17 | +Y; +e | 0.86 | 17 | +Y; +e | 1.026 |
| 5 | +Y | 1.108 | 5 | +Y | 1.328 |
| 18 | +Y; +e | 1.564 | 18 | +Y; +e | 1.095 |
| 13 | -X; +e | 0.893 | 13 | -X; +e | 0.976 |
| 3 | -X | 0.888 | 3 | -X | 0.965 |
| 14 | -X; -e | 0.878 | 14 | -X; -e | 0.953 |
| 22 | -Y; -e | 0.68 | 22 | -Y; -e | 1.004 |
| 7 | -Y | 1.038 | 7 | -Y | 1.245 |
| 21 | -Y; +e | 0.787 | 21 | -Y; +e | 0.932 |
| 10 | +X; -e | 0.969 | 10 | +X; -e | 0.949 |

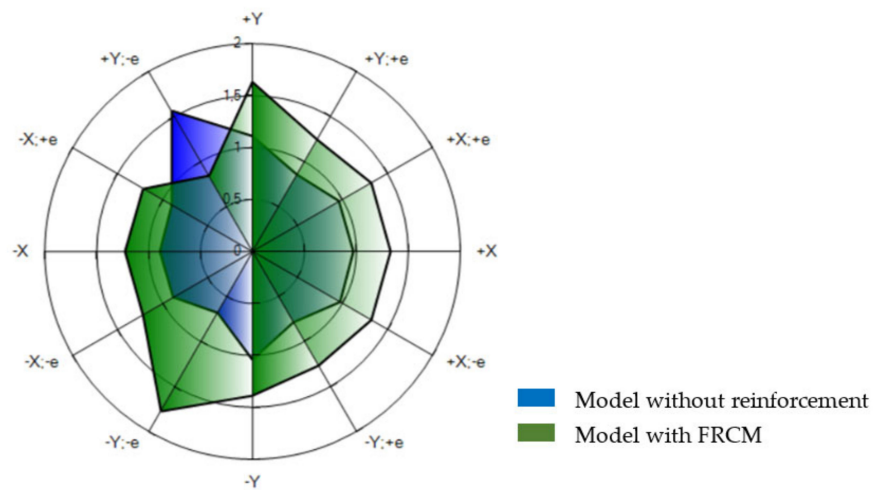


Figure 37. Graphical comparison between model without/with FRCM reinforcement.

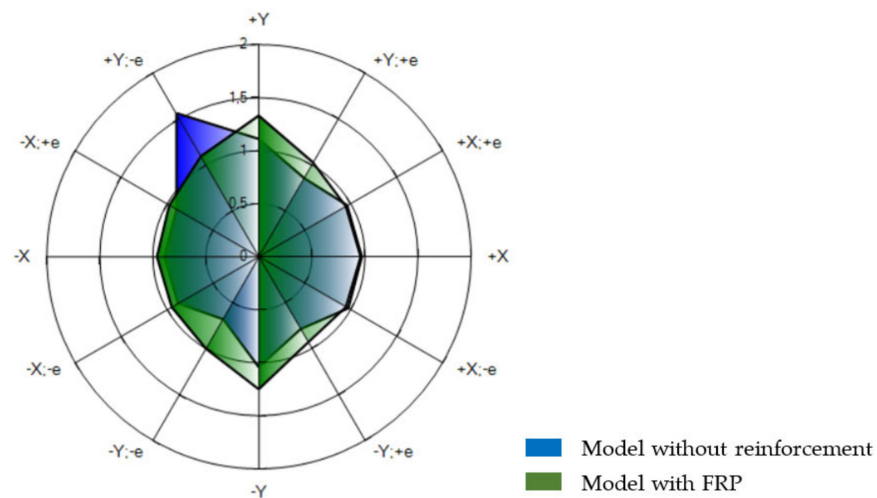
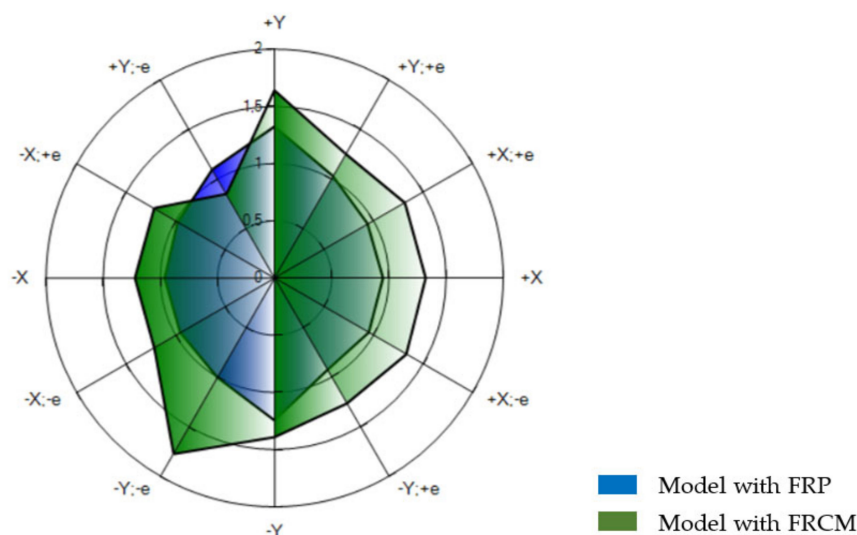


Figure 38. Graphical comparison between model without or with FRP reinforcement.

In conclusion, in Table 13 and Figure 39, the same comparison, both with numerical and graphical representation, between the two reinforced models is provided. In this case, it is possible to underline that the use of an FRP system allows to obtain a higher α index and a better behaviour for the masonry school building in almost all directions.

Table 13. Comparison in terms of α between two reinforced models.

| Model with FRCM | | | Model with FRP | | |
|----------------------------|-----------|----------------|----------------------------|-----------|----------------|
| $\alpha_{SLV,min} = 0.843$ | | | $\alpha_{SLV,min} = 0.932$ | | |
| Nr | Direction | α_{SLV} | Nr | Direction | α_{SLV} |
| 1 | +X | 1.324 | 1 | +X | 0.954 |
| 9 | +X; +e | 1.316 | 9 | +X; +e | 0.941 |
| 17 | +Y; +e | 1.249 | 17 | +Y; +e | 1.026 |
| 5 | +Y | 1.637 | 5 | +Y | 1.328 |
| 18 | +Y, +e | 0.843 | 18 | +Y, +e | 1.095 |
| 13 | -X; +e | 1.215 | 13 | -X; +e | 0.976 |
| 3 | -X | 1.226 | 3 | -X | 0.965 |
| 14 | -X; -e | 1.217 | 14 | -X; -e | 0.953 |
| 22 | -Y; -e | 1.772 | 22 | -Y; -e | 1.004 |
| 7 | -Y | 1.387 | 7 | -Y | 1.245 |
| 21 | -Y; +e | 1.264 | 21 | -Y; +e | 0.932 |
| 10 | +X; -e | 1.324 | 10 | +X; -e | 0.949 |

**Figure 39.** Graphical comparison between two reinforced models.

For both systems, FRP and FRCM, the seismic risk index is not higher than the same in the initial state for all the load combinations and directions. This condition is acceptable since our goal was to obtain the seismic improvement and not the complete upgrading of the structure.

The NTC 18, concerning structural consolidation interventions, establishes that:

“The safety assessment and the intervention project will have to be extended to all parts of the structure potentially affected by behaviour changes, as well as to the structure as a whole [...] unless specific situations relating to cultural heritage, for class III buildings for school use and class IV the value of ζ_E , following the upgrading interventions, must, in any case, be not less than 0.6”.

For the selected interventions with FRP and FRCM systems, the minimum seismic safety factor of 0.6 is attained, thus confirming in both cases the seismic upgrading of the school building. Moreover, the FRP allows to increase more the seismic safety of the structure in direction y. In terms of seismic classification, while an FRCM system can improve the seismic risk of one class, so as to attain a building’s seismic upgrading, an FRP system allows to pass from class C to class A, an improvement of two classes for the seismic risk and, therefore, achieve the seismic retrofitting of the school according to the Italian Guidelines on seismic risk classification of existing buildings. However, this comparison

between solutions should be made also in terms of intervention costs. In fact, while seismic upgrading by FRCM systems is achieved with a cost of about EUR 69.000,00, the seismic retrofitting given by FRP to the masonry building involves the highest intervention cost, equal to about EUR 90.000,00.

5. Conclusions

The current work proposed, through a seismic vulnerability analysis of a masonry school building in the district of Naples, a comparison between FRP and FRCM as retrofitting systems of existing historical heritage constructions.

After providing some information about the main features of the building, the experimental campaign on materials, useful for establishing the state of decay of the construction, was illustrated through description of in situ tests.

Subsequently, a vulnerability analysis conducted according to the current Italian technical standards was performed to evaluate the building safety against both vertical and seismic actions, the latter evaluating both global and local collapse mechanisms.

Since the results of global seismic analysis showed a deficient behaviour of the structure, with α_{SLV} indices, defined as the ratio between the capacity PGA and the demand one, close to 0.6, appropriate structural consolidation operations were designed.

Specifically, the design strategy involved two retrofit techniques: one consisting of the application of Carbon-FRP systems and another based on the use of Glass-FRCM systems.

The results of the seismic non-linear analysis performed on the strengthened FEM model of the school building allowed to attain the seismic upgrading of the inspected masonry structure. In particular, between the two examined retrofitting systems, a better behaviour of the building was noticed in direction y with the application of FRP systems. Moreover, also in terms of seismic risk classification, the FRP-based technique proved to be much more effective than the FRCM-based one, since the passage of two classes, instead of the single one achieved with FRCM systems, was obtained. Nevertheless, this outcome was also dictated by the different intervention costs. In fact, the intervention with FRP-based systems was revealed to be more expensive by about 30% than the one performed with the FRCM technique.

Author Contributions: Conceptualization, A.F.; methodology, A.F.; software, A.P.P.; validation, G.L.; formal analysis, A.P.P.; investigation, A.P.P.; resources, A.P.P.; data curation, G.L. and A.F.; writing—original draft preparation, A.P.P.; writing—review and editing, G.L. and A.F.; visualization, G.L.; supervision, A.F.; project administration, A.F. All authors have read and agreed to the published version of the manuscript.

Funding: This research received no external funding.

Data Availability Statement: The data supporting reported results can be obtained from the authors upon request.

Acknowledgments: The authors would like to acknowledge the DPC-ReLUIS research project, where the current research activity is developed. Also, the contribution of Domenico Brigante, Technical Director of the Olympus Srl company, is gratefully acknowledged.

Conflicts of Interest: The authors declare no conflict of interest.

References

1. Brigante, D. *Structural Consolidation with Composite Materials. Reinforcement with FRP, FRCM e CRM Systems*, 1st ed.; Grafill: Palermo, Italy, 2020. (In Italian)
2. *CNR-DT 200 R1*; Instructions for the Design, Execution and Control of Static Consolidation Interventions through the use of Fiber-reinforced Composites with Inorganic Matrix. Italian Research National Council: Rome, Italy, 2013. (In Italian)
3. Amato, G.; Chen, J.F.; D'Anna, J.; La Mendola, L.; Minafò, G. FRCM Systems for Strengthening Masonry Structures. In Proceedings of the 8th Biennial Conference on Advanced Composites in Construction, Sheffield, UK, 5–7 September 2017.
4. Bertolesi, E.; Grande, E.; Milani, G. Numerical modeling of the bond behaviour of FRCM systems externally applied to masonry substrates. *J. Build. Pathol. Rehabil.* **2019**, *4*, 4. [[CrossRef](#)]

5. Carozzi, G.; Milani, G.; Poggi, C. Mechanical properties and numerical modeling of Fabric Reinforced Cementitious Matrix (FRCM) systems for strengthening of masonry structures. *Compos. Struct.* **2014**, *107*, 711–725. [[CrossRef](#)]
6. D’Antino, T.; Sneed, L.H.; Carloni, C.; Pellegrino, C. Influence of the substrate characteristics on the bond behavior of PBO FRCM-concrete joints. *Constr. Build. Mater.* **2015**, *101*, 838–850. [[CrossRef](#)]
7. Grande, E.; Imbimbo, M.; Sacco, E. Bond behaviour of CFRP laminates glued on clay bricks: Experimental and numerical study. *Compos. Part B Eng.* **2011**, *42*, 330–340. [[CrossRef](#)]
8. Grande, E.; Milani, G. Numerical simulation of the tensile behavior of FRCM strengthening systems. *Compos. Part B Eng.* **2020**, *189*, 107886. [[CrossRef](#)]
9. Clementi, F.; Formisano, A.; Milani, G.; Mosoarca, M. Behavior of existing structures under earthquakes: Advancements in analysis methods and retrofitting system. *AIP Conf. Proc.* **2022**, *2425*, 360001. [[CrossRef](#)]
10. Monni, F.; Quagliarini, E.; Lenci, S.; Clementi, F. Dry masonry strengthening through basalt fiber ropes: Experimental results versus out-of-plane actions. *Key Eng. Mater.* **2015**, *624*, 584–594. [[CrossRef](#)]
11. Scacco, J.; Ghiassi, B.; Milani, G.; Lourenço, P.B. A fast modeling approach for numerical analysis of unreinforced and FRCM reinforced masonry walls under out-of-plane loading. *Compos. Part B Eng.* **2020**, *180*, 107553. [[CrossRef](#)]
12. Vlachakis, G.; Vlachaki, E.; Lourenço, P.B. Learning from failure: Damage and failure of masonry structures, after the 2017 Lesvos earthquake (Greece). *Eng. Fail. Anal.* **2020**, *117*, 104803. [[CrossRef](#)]
13. Bilgin, H.; Shkodrani, N.; Hysenlliu, M.; Ozmen, H.B.; Isik, E.; Harirchian, E. Damage and performance evaluation of masonry buildings constructed in 1970s during the 2019 Albania earthquakes. *Eng. Fail. Anal.* **2022**, *131*, 105824. [[CrossRef](#)]
14. Petrovic, S.; Kilar, V. Design Considerations for Retrofitting of historic Masonry Structures with externally bonded FRP Systems. *Int. J. Archit. Herit.* **2022**, *16*, 957–976. [[CrossRef](#)]
15. Moretic, A.; Stepinac, M.; Lourenço, P.B. Seismic upgrading of cultural heritage—A case study using an educational building in Croatia from historicism style. *Case Stud. Constr. Mater.* **2022**, *17*, e01183. [[CrossRef](#)]
16. Papanicolaou, C.G.; Triantafillou, T.C.; Karlos, K.; Papathanasiou, M. Textile reinforced mortar (TRM) versus FRP as strengthening material of URM walls: Inplane cyclic loading. *Mater. Struct.* **2007**, *40*, 1081–1097. [[CrossRef](#)]
17. Razavizadeh, A.; Ghiassi, B.; Oliveira, D.V. Bond behavior of SRG-strengthened masonry units: Testing and numerical modeling. *Constr. Build. Mater.* **2014**, *64*, 387–397. [[CrossRef](#)]
18. Sneed, L.H.; D’Antino, T.; Carloni, C.; Pellegrino, C. A comparison of the bond behavior of PBO-FRCM composites determined by double-lap and single-lap shear tests. *Cem. Concr. Compos.* **2015**, *64*, 37–48. [[CrossRef](#)]
19. Ministry of Infrastructure and Transport. *Technical Standards for Construction nr. 42 of 20-2-2018*; (In Italian). Official Gazette: Rome, Italy, 2018.
20. Ministry of Infrastructure and Transport. *Instructions for the Application of the New Technical Code for Constructions nr. 35 of 11-02-2019*; Official Gazette: Rome, Italy, 2019. (In Italian)
21. Lagomarsino, S.; Podestà, S.; Resemini, S.; Curti, E.; Parodi, S. Mechanical models for the seismic vulnerability assessment of churches. In Proceedings of the 4th International Seminar on Structural Analysis of Historical Constructions (SAHC04), Padua, Italy, 10–13 November 2004; Taylor & Francis: London, UK, 2004; Volume 2, pp. 1091–1101.
22. Penna, A.; Lagomarsino, S.; Galasco, A. A nonlinear macroelement model for the seismic analysis of masonry buildings. *Earthq. Eng. Struct. Dyn.* **2014**, *43*, 159–179. [[CrossRef](#)]
23. Ministerial Decree of Infrastructures. *Guidelines for the Seismic Classification of Buildings M. D. 65, 07/03/2017*; (In Italian). Ministry of Infrastructure and Transport: Rome, Italy, 2017.
24. Edilportale. Composite Materials and Application Fields. Available online: https://www.edilportale.com/news/2021/09/focus/cosa-sono-i-materiali-compositi-e-quali-gli-ambiti-di-applicazione_84952_67.html (accessed on 3 June 2022).
25. Ramaglia, G.; Crisci, G.; Fabbrocino, F.; Lignola, G.L.; Prota, A. FRP vs FRCM in flexural strengthening of masonry. In Proceedings of the SMAR 2019, 5th Conference on Smart Monitoring, Assessment and Rehabilitation of Civil Structures, Potsdam, Germany, 27–29 August 2019.
26. Estevan, L.; Baeza, F.J.; Bru, D.; Ivorra, S. Stone masonry confinement with FRP and FRCM composites. *Constr. Build. Mater.* **2020**, *237*, 117612. [[CrossRef](#)]